Eric L. Wisotzky*, Anna Hilsmann, and Peter Eisert

3D Hyperspectral Light-Field Imaging: a first intraoperative implementation

https://doi.org/10.1515/cdbme-2023-1153

Abstract: Hyperspectral imaging is an emerging technology that has gained significant attention in the medical field due to its ability to provide precise and accurate imaging of biological tissues. The current methods of hyperspectral imaging, such as filter-wheel, snapshot, line-scanning, and push-broom cameras have limitations such as low spatial and spectral resolution, slow acquisition time. New developments on the field of light field cameras show the potential to overcome these limitations. In this paper, we use a novel hyperspectral light-field camera and try to combine the capability of hyperspectral and 3D analysis. For this purpose we calibrate our system and test it during two ENT-surgeries to show its potential for improving surgical outcomes. The micro-lenses of the camera map 66 spectral sub-images onto the sensor allowing to reconstruct the spectral behavior of the captured scene in the spectral range of 350-1000nm. In addition, we use the sensor data to apply a 3D camera calibration pipeline to allow 3D surface reconstruction. We captured 26 calibration images and achieved calibration results in accordance to stated company data. The best calibration showed a re-projection error of 0.55 px. Further, we tested the camera during a parotidectomy and a neck-dissection. The extracted reflectance spectra of the selected venal and arterial regions correspond perfectly to the spectrum of oxygenated and deoxygenated hemoglobin. For the first time, up to our knowledge, a hyperspectral light-field camera has been used during a surgery. We were able to continuously capture images and analyze the reconstructed spectra of specific tissue types. Further, we are able to use the sensor data of the micro-lens projections to calibrate the multi-lens camera system for later intraoperative measurement tasks.

Keywords: Hyperspectral Imaging, Light field imaging, 3D reconstruction, Stereo calibration, Tissue analysis.

1 Introduction

Hyperspectral imaging is an emerging technology that has gained significant attention in the medical field due to its ability to provide precise and accurate imaging of biological tissues [2, 6]. In surgical applications, hyperspectral imaging can aid in the identification and differentiation of tissues, leading to improved surgical outcomes [2, 17]. The current used methods of hyperspectral imaging, such as filter-wheel, snapshot, line-scanning, and push-broom cameras [3, 5, 8], have limitations such as low spatial and spectral resolution, slow acquisition time, and/or inability to capture light fields [11].

New developments on the field of light field cameras show the potential to overcome these limitations. A light field camera captures information by using an array of micro-lenses placed in front of the sensor, which allows the camera to capture multiple views of the same scene simultaneously. This information can then be used to create images with different focus points, as well as to generate 3D images and videos with the ability to change the point of view after the image has been captured.

In the context of hyperspectral imaging, capturing the light field in addition to the spectral information can provide additional information about the optical properties of the tissue being imaged, which can be useful in surgical applications.

In this paper, we use a novel hyperspectral light-field camera and try to combine the capability of hyperspectral and 3D analysis. For this purpose we calibrate our system and test it time during two surgeries to show its potential for improving surgical outcomes.

2 Materials and Methods

2.1 Setup

In this work, we use a spectral snapshot light-field camera[1], see Fig. 1. The technical specifications of the system are summarized in Tab. 1. The system is connected to a laptop[2] via Ethernet and the data are captured with 1 fps. For calibration a working distance (WD) of about $d_{calib} \approx 26$cm is used. Intraoperative imaging is performed with WD of about $d_{OR} \approx 35$cm.

***Corresponding author: Eric L. Wisotzky, Peter Eisert,** Fraunhofer Heinrich-Hertz-Institute HHI & Humboldt-University, Berlin, Germany, e-mail: eric.wisotzky@hhi.fraunhofer.de
Anna Hilsmann, Fraunhofer Heinrich-Hertz-Institute HHI, Berlin, Germany

1 Cubert GmbH, Ulm, Germany
2 DELL Precision 5570

Fig. 1: The hyperspectral light-field camera used in this work. Behind each micro-lens a different spectral filter ($\lambda = 350 - 1000$nm) is located.

Tab. 1: The technical specifications of the used light-field camera system.

Parameter	Value
Sensor	CMOS
Sensor ADC	12 bits
Sensor resolution	5120×3840 px
Output resolution	410×410 px
Sensor size	32.8×24.6 mm
Pixel size	6.4×6.4 μm
Spectral range	$350 - 1002$ nm
No. of spectral bands	164
Field of view (FOV)	35 deg
No. of micro-lenses	66
Filter transmission	$> 90\%$
Band width (FWHM avg.)	10 nm
Spectral resolution	4 nm
Camera dimension	$60 \times 60 \times 57$ mm
Camera weight	350 g

2.2 3D-Calibration

The micro-lenses of the camera map 66 spectral sub-images onto the sensor. To perform a camera calibration for exact 3D scene reconstruction, at least two central sub-images, e.g., 730nm and 740nm, have to be used. Then, for 3D reconstruction only the sub-images used in calibration are valid. The more sub-images are included in the calibration, the more information can be used for scene reconstruction.

For the calibration purpose, a checkerboard is used due to the widely acceptance in camera calibration [1, 9, 10, 13]. The checkerboard consists of two dots in the center to determine the individual quadrants of the board for a better model initialization. It is captured from different view angles and WDs. Fig. 2 shows the calibration setup. To achieve acceptable results, we upsampled the sub-images from 470×470 pixels by factor 4 to a size of 1880×1880 pixels. The overall calibration process is described in detail in [10, 13, 15] and consists of five steps

1. Feature detection
2. Sub-image pre-calibration
3. Single sub-image calibration
4. Stereo calibration over individual sub-image pairs
5. Validate calibration.

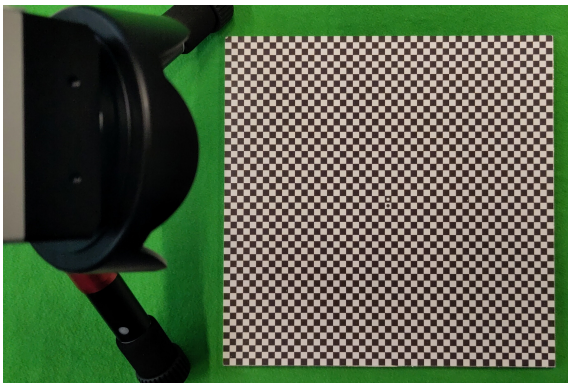

Fig. 2: The used calibration setup. The checkerboard consists of two dots in the center to determine the individual quadrants of the board. It is captured from different angles and rotations.

The 2D feature detection is performed for all captured checkerboard images on all upsampled sub-images [18]. The detected 2D features are mapped to the reference 3D model features to derive the approximate sub-image pose. Each feature correspondence gets a unique ID for a detailed 2D-3D evaluation. Then for each sub-image, the intrinsic camera parameter are calculated by gradient descent to determine focal length and lens distortion. Here we assume, that each sub-image has the same focus length. Next, based on the intrinsic camera parameters, the relative sub-image pose between the two analyzed sub-images is computed. This procedure up to this point does not use all captured calibration images. Some are used for the final validation step to verify the system on 'unseen' images.

The validation criteria are (1) the distance survey of 3D reconstructed features and (2) the planarity of the 3D reconstructed calibration target. A successful calibrated system enables to perform image-based measurements if reliable sub-pixel correspondence in the two sub-images are found. The system has been tested at two Ear-Nose-Throat surgeries.

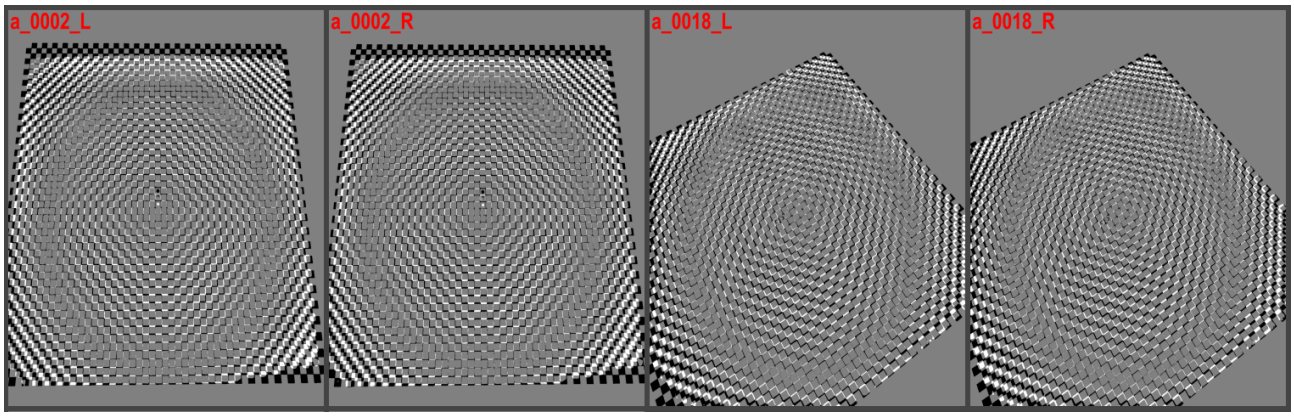

Fig. 3: An example of difference images between the projected ground truth checkerboard data and two sub-images ('L' and 'R') for two different captured calibration images (0002 and 0018).

3 Results

We captured 26 images, where the same checkerboard is visible from different angles and rotations. We performed the described calibration process ten times. In comparison to the optically measured lens-to-lens distance (center-to-center) of $d \approx 3$mm, we achieved $d = 2.8-3.3$mm during the performed calibrations. Further, a reasonable focal length could be achieved. We calculated α in the range of $\alpha = 2260 - 2296$px, which results in a focal length of $f = 14.46 - 14.69$.

The best calibration run showed a 3D planarity of 1.09 mm, cf. Fig. 3, and a stereo re-projection error of 0.55 px after the validation step, cf. Fig. 4.

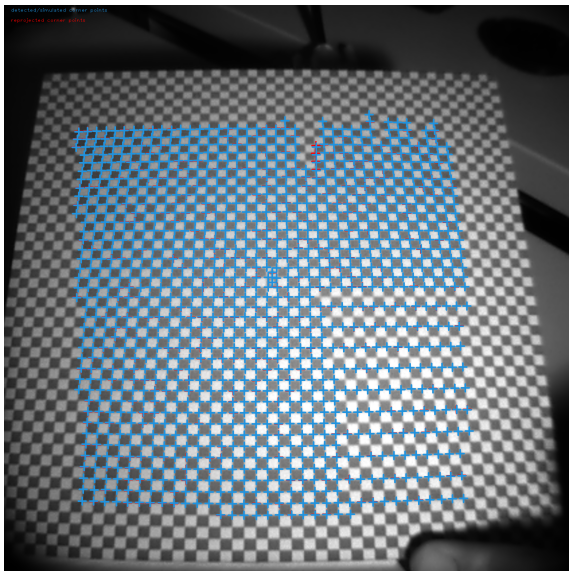

Fig. 4: An example of the re-projected corner points of the checkerboard. The detected corner points (blue) fit almost perfectly with the re-projected corner points.

Figure 5 shows a camera view of spectral band $\lambda = 750$nm of our intraopertaive capturing during a neck dissection at the Charité – Universitätsmedizin Berlin. The extracted reflectance and absorption spectra of the selected venal and arterial regions correspond perfectly to the spectrum of oxygenated and deoxygenated hemoglobin in literature [4].

4 Discussion and Conclusion

For the first time, up to our knowledge, a hyperspectral light-field camera has been used during a surgery. We were able to continuously capture images and analyze the reconstructed spectra of specific tissue types. Further, we are able to use the sensor data of the micro-lens projections to calibrate the multi-lens camera system for later intraoperative measurement tasks.

All calibration results are in accordance of Michels et al. [7]. This leads us to believe that such a novel hyperspectral light field camera has high application potential in intraoperative decision making. Therefore, we plan to compare this system with other multispectral as well as hyperspectral systems [12, 14, 16].

Acknowledgment: We would like to thank Cubert GmbH, Ulm, Germany for the possibility to access the raw sensor data.

Author Statement

Research funding: The author state no funding involved. Conflict of interest: Authors state no conflict of interest. Informed consent: Informed consent has been obtained from all individuals included in this study. Ethical approval: The research related to human use complies with all the relevant national regulations, institutional policies and was performed in accordance with the tenets of the Helsinki Declaration, and has been

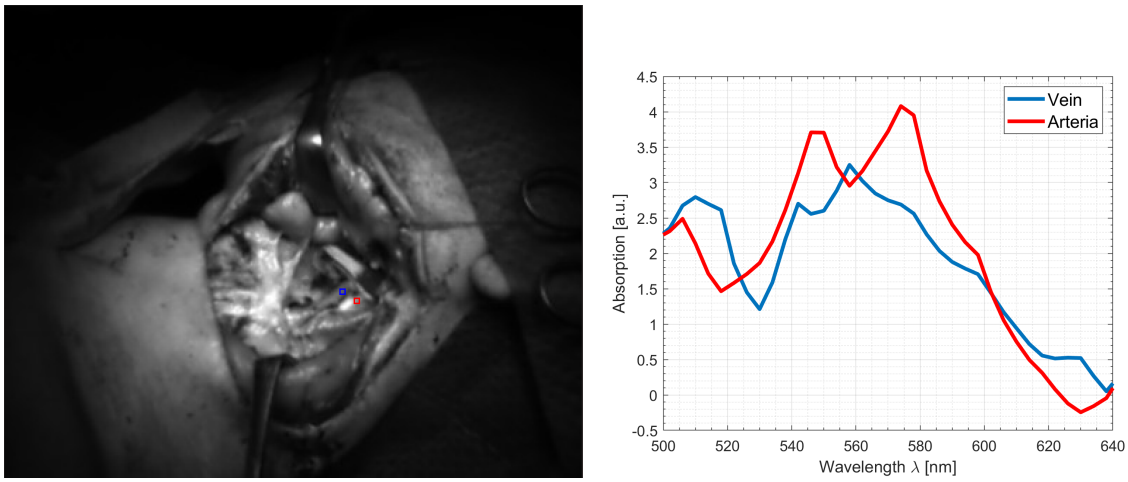

Fig. 5: Left: The camera view for one surgical test during a neck dissection. One vein (blue) and the arteria (red) are marked in the center of the image. Right: The reconstructed spectral absorption curves of the marked tissues in the range of $\lambda = 500 - 640$nm. Both spectra correspond very well to the well known spectra of oxygenated and deoxygenated hemoglobin [4].

approved by the authors' institutional review board or equivalent committee.

References

[1] Allan M, Mcleod J, Wang C, Rosenthal JC, Hu Z, Gard N, et al. Stereo correspondence and reconstruction of endoscopic data challenge. arXiv preprint, 2021, arXiv:2101.01133.

[2] Clancy NT, Jones G, Maier-Hein L, Elson DS, Stoyanov D. Surgical spectral imaging. Med Image Anal, 2020, 63:101699.

[3] Clancy NT, Soares AS, Bano S, Lovat LB, Chand M, Stoyanov D. Intraoperative colon perfusion assessment using multispectral imaging. Biomed Opt Express, 2021, 12(12):7556-7567.

[4] Dervieux E, Bodinier Q, Uhring W, Théron M. Measuring hemoglobin spectra: searching for carbamino-hemoglobin. J Biomed Opt, 2020, 25(10):105001.

[5] Ebner M, Nabavi E, Shapey J, Xie Y, Liebmann F, Spirig JM, et al. Intraoperative hyperspectral label-free imaging: from system design to first-in-patient translation. J Phys D: Appl Phys, 2021, 54(29):294003.

[6] Lu G, Fei B. Medical hyperspectral imaging: a review. J Biomed Opt, 2014, 19(1):010901.

[7] Michels R, Brandes AR. Multilinsen-Kamerasystem und Verfahren zur hyperspektralen Aufnahme von Bildern. Pat DE102019008472A1, 2019

[8] Mühle R, Markgraf W, Hilsmann A, Malberg H, Eisert P, Wisotzky EL. Comparison of different spectral cameras for image-guided organ transplantation. J Biomed Opt, 2021, 26(7):076007.

[9] Rosenthal JC, Gard N, Schneider A, Eisert P. Kalibrierung stereoskopischer Systeme für medizinische Messaufgaben. 16th Annual CURAC Conference. PZH-Verlag, 2017

[10] Rosenthal JC, Wisotzky EL, Matuschek C, Hobl M, Hilsmann A, Eisert P, Uecker FC. Endoscopic measurement of nasal septum perforations. HNO, 2022 70(S1):1-7. doi: 10.1007/s00106-021-01102-4

[11] Shapey J, Xie Y, Nabavi E, Bradford R, Saeed SR, Ourselin S, Vercauteren T. Intraoperative multispectral and hyperspectral label-free imaging: A systematic review of in vivo clinical studies. J Biophotonics, 2019, 12(9):e201800455.

[12] Wisotzky EL, Kossack B, Uecker FC, Arens P, Hilsmann A, Eisert P. Validation of two techniques for intraoperative hyperspectral human tissue determination. J Med Imaging, 2020, 7(6):065001.

[13] Wisotzky EL, Rosenthal JC, Eisert P, Hilsmann A, Schmid F, Bauer M, et al. Interactive and multimodal-based augmented reality for remote assistance using a digital surgical microscope. Conference on Virtual Reality and 3D User Interfaces (VR). IEEE, 2019, pp. 1477-1484.

[14] Wisotzky EL, Rosenthal JC, Hilsmann A, Eisert P, Uecker FC. A multispectral 3D-endoscope for cholesteatoma removal. Curr Dir Biomed Eng, 2020, 6(3):257-260.

[15] Wisotzky EL, Rosenthal JC, Meij S, van den Dobblesteen JJ, Arens P, Hilsmann A, et al. Telepresence for surgical assistance and training using eXtended reality (during and after pandemic periods). J Telemed Telecare, 2023, in publication. doi: 10.1177/1357633X231166226

[16] Wisotzky EL, Rosenthal JC, Wege U, Hilsmann A, Eisert P, Uecker FC. Surgical guidance for removal of cholesteatoma using a multispectral 3D-endoscope. Sensors, 2020, 20(18):5334.

[17] Wisotzky EL, Uecker FC, Arens P, Dommerich S, Hilsmann A, Eisert P. Intraoperative hyperspectral determination of human tissue properties. J Biomed Opt, 2018, 23(9):091409.

[18] Zilly F, Müller M, Eisert P, Kauff P. The stereoscopic analyzer—an image-based assistance tool for stereo shooting and 3D production. International Conference on Image Processing (ICIP). IEEE, 2010, pp. 4029-4032.